THE ASTRONOMICAL JOURNAL, 122:1051–1066, 2001 August

THE STRUCTURE OF THE KUIPER BELT: SIZE DISTRIBUTION AND RADIAL EXTENT

BRETT GLADMAN[1]
Departement Cassini, Observatoire de la Côte d'Azur, B.P. 4229, F-06304 Nice Cedex 4, France; gladman@obs-nice.fr
J. J. KAVELAARS[1]
Department of Physics and Astronomy, McMaster University, Hamilton, ON L8S 4M1, Canada; kavelaars@physics.mcmaster.ca
JEAN-MARC PETIT AND ALESSANDRO MORBIDELLI[1]
Departement Cassini, Observatoire de la Côte d'Azur, B.P. 4229, F-06304 Nice Cedex 4, France; petit@obs-nice.fr
MATTHEW J. HOLMAN[1]
Harvard-Smithsonian Center for Astrophysics, 60 Garden Street, Cambridge, MA 02138; mholman@cfa.harvard.edu
AND
T. LOREDO
Department of Astronomy, Cornell University, Ithaca, NY 14853; loredo@astrosun.tn.cornell.edu
Received 2000 September 24; accepted 2001 May 9

ABSTRACT

The size distribution in the Kuiper Belt records physical processes operating during the formation and subsequent evolution of the solar system. This paper reports a study of the apparent magnitude distribution of faint objects in the Kuiper Belt, obtained via deep imaging on the Canada-France-Hawaii Telescope and the ESO Very Large Telescope UT1. We find that the entire range of observed objects (magnitudes $m_R \sim 20$–27) is well represented by an unbroken power law, with the number of objects per square degree brighter than magnitude R being of the form $\Sigma(m_R < R) = 10^{\alpha(R-R_0)}$, with $\alpha = 0.69$ and $R_0 = 23.5$. This luminosity function's slope implies a steep size distribution in the observed range, which should "roll over" to a shallower "collisional" slope once observations extend to even fainter magnitudes and thus sample bodies whose collisional ages become less than the age of the solar system. Our observations indicate the roll over is for diameters of less than 50 km, in agreement with collisional models. Modeling our survey gives a belt mass between 30 and 50 AU of order 0.1 $M_\oplus$, relatively insensitive to the roll over diameter as long as the latter is $\gtrsim$1 km. We report the discovery of several objects outside of 48 AU and discuss the evidence for a sharp outer edge to the trans-Neptunian distribution.

Key words: comets: general — Kuiper belt

1. INTRODUCTION

The trans-Neptunian region preserves valuable clues regarding the formation of the outer solar system, encoded in the still poorly known orbital distribution, in the size distribution of its members, and in the chemical properties of these trans-Neptunian objects (TNOs). Once determined, these data, in combination with more fully developed theoretical models on accretional evolution, will provide powerful constraints on how the giant planets formed. The conclusions that can be drawn from presently available information are cloudy, but this accurately represents the current state of this exciting field of research (Jewitt & Luu 2000).

This paper combines theoretical and observational considerations about the spatial/orbital and size distributions of known trans-Neptunian objects with results of our observational program to better determine these quantities. Sections 2 and 3 present the theoretical framework. Although focusing mainly on our deep imaging surveys, we also indicate where our ongoing recovery campaign has yielded new insights into the belt's structure. The reader who is interested mainly in the observational results is encouraged to jump to § 4, although insightful interpretation of these observations requires an understanding of the present theoretical context of the field.

2. ORBITAL STRUCTURES OUTSIDE NEPTUNE

We begin by describing orbital groupings (Fig. 1) in the TNO region, some of which only exist as concepts, others of which are well populated.

1. *The "classical belt" between* 40 *and* 48 AU is so named (Jewitt, Luu, & Trujillo 1998) because it most resembles the Kuiper Belt that was originally searched for: a belt of dynamically cold (low e and i) objects outside Neptune representing the leftover planetesimal disk, which never succeeded in accreting into planetary-sized bodies. However, the mass currently between 30 and 50 AU is 2 to 3 orders of magnitude below expectations (see § 3). Gravitational erosion over the solar system's lifetime (Duncan, Levison, & Budd 1995) clears out certain regions, in particular the prominent gap between 40 and 42 AU, but cannot alone account for the mass loss if the TNO population has not been affected by some other strong perturbative process that pushed most of the mass to unstable orbits. The dynamical excitation (departure from $e = i = 0$ orbits) in the region is much larger than was expected. The known e and i distributions likely indicate only a lower limit to the original excitation. First, the eccentricity (e) distribution is truncated by the Neptune-approaching limit of pericenters $q = a(1 - e) < 35$ AU (Torbett & Smoluchowski 1990); most TNOs initially above this line (Fig. 1*b*) were eliminated by Neptune. Therefore the *inclination* (i) distribution

[1] Visiting Astronomer, Canada-France-Hawaii Telescope, which is operated by the National Research Council of Canada, the Centre National de la Recherche Scientifique of France, and the University of Hawaii. Data from VLT from observations collected at the European Southern Observatory, Chile, proposal 63.S-0121A.

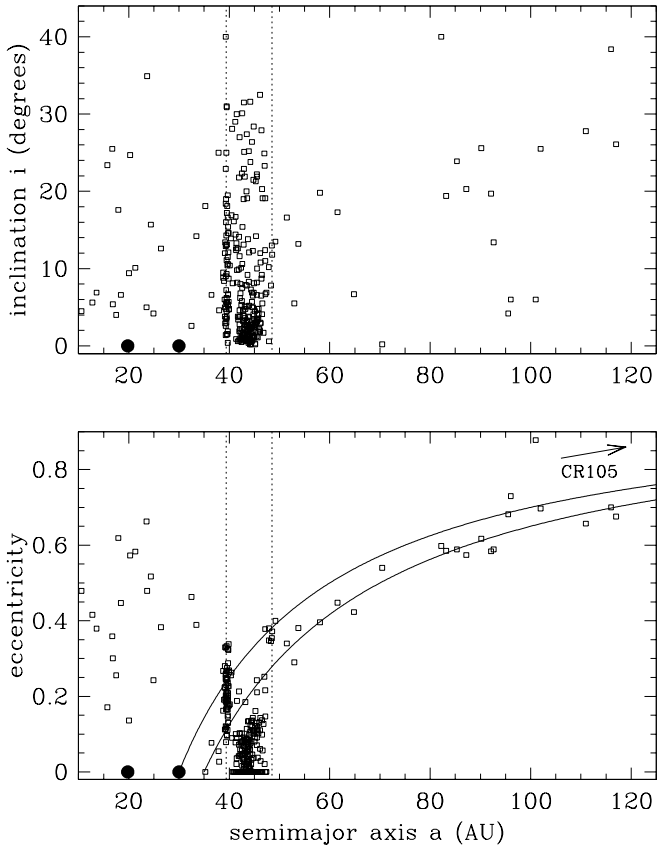

FIG. 1.—Orbital distribution of TNOs in the MPC database as of 2000 July 3. All orbits have been included (even those with as little as 24 hr arcs). For reference, we show the distances of Uranus and Neptune (*heavy dots*), vertical lines at the 3:2 (39.4 AU) and 2:1 (47.8 AU) resonances with Neptune, and curves in the bottom panel marking perihelion distances of 30 and 35 AU. The arrow points toward the elements of 2000 CR_{105} at (a, e, i) = (675, 0.940, 23°).

is more primordial and gives a better measure of the region's dynamical perturbation; however, the i-distribution of detected TNOs is biased toward low inclinations because most TNO surveys focus on the ecliptic, in which high-i TNOs spend little time (Jewitt, Luu, & Chen 1996; Kavelaars et al. 2001). In contrast, the brightening as TNOs approach pericenter means that there is a bias toward finding high-e TNOs (see also Allen, Bernstein, & Malhotra 2001); this is probably a minor effect compared with the truncation of the high-e distribution due to Neptune crossing. Taking the currently known TNOs with $30 < a < 55$ and eliminating the provisional $e = 0$ orbits, we find an rms excitation $[(e^2 + i^2)^{1/2}]$ of 0.23, which we take as a lower limit to the classical belt's velocity excitation. The currently observed 100–1000 km objects could never have accreted in this velocity environment (see below); a violent event has affected this region.

2. *Plutinos* are trapped, like Pluto (Cohen & Hubbard 1965), in the 3:2 mean motion resonance with Neptune. Some Plutinos have $q < 35$ AU (Fig. 1*b*), but the resonance prevents close encounters (see, e.g., Malhotra 1996). Uranus crossing truncates the distribution at $e \sim 0.4$. The interior of the resonance is dynamically stable over the age of the solar system, although Morbidelli (1997) showed that Plutinos with large libration amplitude escape by dynamical diffusion on gigayear timescales. The origin of Plutinos will be discussed below. There are other TNOs in resonances throughout the region (Morbidelli, Thomas, & Moons 1995; Malhotra 1996) with similar dynamical properties, which can collectively be called the "resonant population" (see also Trujillo, Jewitt, & Luu 2000), although we single out the 2:1 for special consideration below.

3. *TNOs with* $a = 36$–39 AU *and small* e *and* i ($\lesssim 0.05$) are predicted to be stable by Duncan et al. (1995). Prior to mid-1999, no TNOs except for 1995 DA_2 (protected in the 4:3 resonance) were known to be in this region, potentially implying that the dynamical processes that sculpted the belt left nothing in this small stable region of phase space. Our 1999 September recovery (MPEC 1999-X02) of 1998 SN_{165} (discovered by Spacewatch) implied that it inhabited this region, and our 2000 July recovery confirmed this ($a = 38.1$, $e = 0.05$, $i = 5°$). The TNO 1998 HN_{151} ($a = 37.9$, $e = 0.06$, $i = 25°$) may also be dynamically stable, according to the map of Duncan et al. (1995). The nomenclature problem for the classical belt posed by this population is discussed in Gladman (2001).

4. *Objects in the* 2:1 *resonance* at $a = 47.8$ AU were also not identified until early 1999. However, continued observations of *previously discovered* TNOs 1997 SZ_{10} and 1996 TR_{66} showed them to be near the resonance, and several objects discovered in 1999–2000 have been given (assumed) nearly resonant 2:1 orbits. Waiting for recoveries would be prudent, as 1996 TR_{66} was placed in the resonance upon its 1998 recovery (Levison & Malhotra 1998), but recent observations have moved its current orbit just outside the resonance (Nesvorný & Roig 2001). 1997 SZ_{10}'s 1999 elements placed it in an unstable portion of the 2:1, but our recovery of it in 2000 September (MPEC 2000-S55) showed it to be firmly inside the resonance, as predicted by Nesvorný & Roig (2001). Being the most distant first-order mean motion resonance, the 2:1 serves as natural division between the "inner" Kuiper Belt (the only observed portion up to 1999) and the "outer" Kuiper Belt. This resonance also figures prominently in some formation scenarios, and hence we propose to use its heliocentric distance of 48 AU as a dividing line between the "inner" and "outer" Kuiper Belt.

5. *Low-e TNOs with* $a > 48$ AU do not exist in the current Minor Planet Center (MPC) orbital database. Even in 1998 there were a few objects in the database whose orbits penetrated the region beyond 48 AU, and thus there was never any question that objects existed outside this *heliocentric distance*; the issue was whether flux-limited surveys with their inherent bias to the nearest objects should have found them and/or a population of low-e objects with $a > 48$ AU. Dones (1997) and Jewitt et al. (1998, hereafter JLT98) modeled the available data and concluded that surveys should have detected such objects if they existed. Gladman et al. (1998, hereafter G98) Chiang & Brown (1999, hereafter CB99) showed that if the steeper luminosity function favored by the G98 analysis was used, then the nondetection of objects outside $\Delta = 50$ AU was not significant; we switch to a dividing line of 48 AU hereafter, for the reason just cited above. Hahn (2000) proposed that the disk outside 48 AU is extremely dynamically cold, confined to the invariable plane (not the ecliptic), and thus has escaped detection, but preventing the dynamical excitation dramatically seen interior to 48 AU from reaching slightly outside the 2:1 resonance seems rather problematic. Between the beginning of 1999 and the time of writing, ~ 10 objects have been detected outside of a *distance* of 48

AU, four of which we report below. We will discuss the issue of whether they actually have *semimajor axes* outside 48 AU and/or low eccentricities below, but at this date none can be proved to be in this class.

6. *Scattered-disk objects* are those that have highly eccentric orbits outside Neptune, although no firm definition appears to exist (see Gladman 2001 for discussion). Supply sources that could populate this structure are comets that have escaped from the Kuiper Belt to Neptune-encountering orbits, or that were emplaced there *primordially* as the giant planets cleared the outer solar system of leftover planetesimals (Levison & Duncan 1997; Guillot & Gladman 2000). The first such object identified was 1996 TL_{66} (Luu et al. 1997), but it appears likely that many of the TNOs discovered before 1998 and now lost may have been on highly eccentric orbits. Further work is warranted in developing models that self-consistently produce the correct Oort cloud and scattered populations; unfortunately, this may require knowing how the giant planets formed!

7. *Centaurs inside* 30 AU represent the transition population between the short-period comets and their source region outside of 30 AU. More modern terminology is that almost all the Centaurs belong to the "ecliptic comet" population (Levison 1996) whose flattened orbital distribution indicates a nonspherical source. For a Kuiper Belt source, proposed supply mechanisms include long-term dynamical instabilities (Levison & Duncan 1993; Holman & Wisdom 1993; Duncan et al. 1995; Levison & Duncan 1997; Morbidelli 1997; Nesvorný & Roig 2001) or collisions (Davis & Farinella 1997). Coming more into favor is the idea that the "scattered disk" is sufficiently populated at the current epoch for its continuing dynamical erosion to remain capable of producing the required input of Jupiter-family comets and Centaurs (Duncan & Levison 1997). An important advance in the last year has been the identification of two objects: 1999 OX_3, discovered and recovered by us (MPECs 1999-P29, 2000-S12), and 1998 BU_{48}, discovered by Spacewatch and recovered at Lowell Observatory 2 years later (MPEC 2000-E50). These are the first "transition objects" (Gladman 2001) between the TNO population and the Centaur population; both are Neptune-crossing with $a > 30$ AU, but are on orbits not dynamically protected from Neptune by resonant protection mechanisms. Are these to be classified as Centaurs?

3. FORMATION OF THE OUTER SOLAR SYSTEM

The overarching conclusion of our survey of the structure of the TNO region is that the observed portions of the Kuiper Belt are not dynamically cold and that the region has been affected by some strong dynamical process (or processes). This section explores the scenarios which could have done this, with particular attention to the distant Kuiper Belt. Although an understanding of the processes involved is still incomplete, an overall scenario for the formation of the outer solar system proceeds roughly as follows.

After the collapse of a protosolar cloud to a flattened disk surrounding the young Sun, the solid chemical species that could condense in the local physical conditions of the disk did so. In a poorly understood process, the solids clump together to form planetesimals (see, e.g., Beckwith, Henning, & Nakagawa 2000). By the billions, these planetesimals then interact with each other gravitationally and collisionally (Stern & Colwell 1997a; Davis & Farinella 1997; Kenyon & Luu 1999; Davis, Farinella, & Weidenschilling 1999) and accrete together to form larger objects. Even though kilometer-scale and larger TNOs were dynamically decoupled from the gas, while they remained smaller than ~ 100 km the gravitational self-stirring of the distribution was negligible. Call this the *accretional phase* of the TNO region. Models by Kenyon & Luu (1999) rapidly produce $D = 1000$ km bodies and quickly (~ 20–30 Myr) produce a differential size distribution of power-law index $q = 4$ for objects larger than 10 km. In the modeling of Davis et al. (1999), the slope of the size distribution for the bodies larger than several kilometers is always steeper and changes with time (Fig. 2); it is unclear what physics in the modeling produces the difference in the final size distributions seen in these studies. However, in both models a differential size index ($q = 3.5$; Dohnanyi 1969) is obeyed by bodies smaller than some "knee" of steadily increasing diameter, at which the collisional lifetime was comparable to the age of the growing system.

Today's classical belt is strongly dynamically excited (§ 2, paragraph 2), and the relative encounter speeds are currently so large that accretion is impossible. Stern & Colwell (1997b) quantitatively showed that the mass currently estimated to be in the 30–50 AU region is 2 to 3 orders of magnitude below that which is (1) estimated to have been there from a simple extrapolation of the solid mass density represented by the giant planets *and* (2) necessary to have accreted bodies hundreds of kilometers in diameter. A major puzzle in solar system science is to determine the process or processes that produced this mass depletion and excited the orbital distribution. Evidently it is possible (and we believe likely) that a single process did both, but hybrid models exist.

At the epoch when the orbital excitation occurred, the size distribution of large TNOs "froze." Bodies grew no

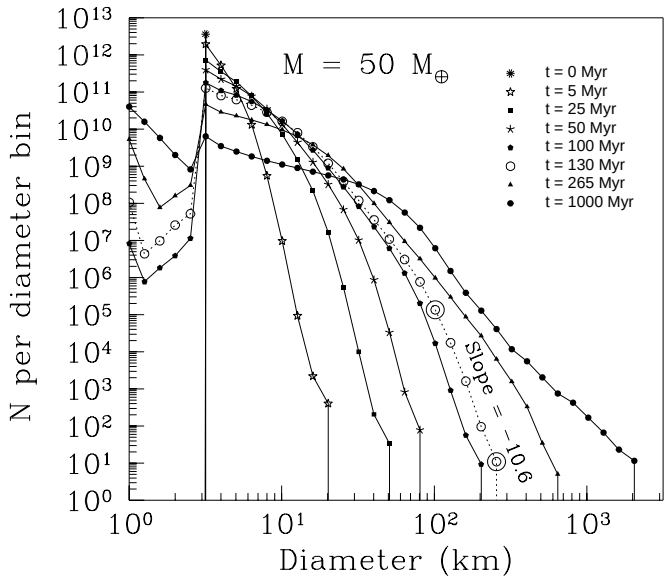

FIG. 2.—Example of the evolution of the size distribution of the TNO region during the accretionary epoch. Beginning with a distribution of $\simeq 3$ km bodies, larger bodies coagulate. The slope at the large size end evolves and is a signature of the duration of the accretion. At each epoch, the steep slope for the large bodies "rolls over" to a shallow collisional equilibrium slope at the size where the collisional lifetime is roughly equal to the age of the population. (Figure from the work of Davis et al. 1999, provided by the authors.)

further, and the continued collisional activity over the age of the solar system caused negligible modifications to the size distribution of sufficiently large bodies. Stern & Colwell (1997b) and Davis & Farinella (1997) independently estimated this critical diameter at ~ 50 km. This turnover point depends on the orbital properties (and hence collision speeds) of the system, TNO strengths, and the number of TNOs of various sizes. TNOs of diameter D(km) with 4% albedos at geocentric distance Δ(AU) obey the scaling

$$m_R \simeq 25.9 + 2.5 \log \left[\left(\frac{\Delta_{\rm AU}}{50} \right)^4 \left(\frac{100}{D_{\rm km}} \right)^2 \right] \qquad (1)$$

near opposition, neglecting phase effects. Bodies of 50 km have magnitudes of $m_R \sim 26.5$ at 40 AU, and thus probing this population in the classical belt is near the limits of current ground-based surveys. Therefore, almost all currently observed TNOs are bigger than the roll over, and their size distribution preserves a record of the large-size planetesimal accretion process. If accretion "shut down early," then this slope could be used in conjunction with accretional models to determine how long planetesimal building lasted in the TNO region.

Some theories for the origin of the dynamical excitation discussed below produce little appreciable mass loss (less than an order of magnitude, say). Models show that the size distribution of bodies smaller than the roll-over point at the end of accretion could be appreciably affected by subsequent collisional erosion. Davis & Farinella (1997) and Stern & Colwell (1997b) showed that considerable mass could then be removed by "collisional grinding," but this requires steep slopes ($q \gtrsim 4.5$) *at the end of accretion* in the size range of the small bodies, so that most of the mass is in the easily disrupted small TNOs. This size distribution is steeper than that predicted to result from the accretional regime, at least for the 1–10 km bodies (Davis et al. 1999; Kenyon & Luu 1999). Much uncertainty remains in these models regarding strengths and absolute number of bodies, so the collisional destruction of most of the mass in an excited TNO distribution with a steep initial size distribution remains a possibility for the mass removal. However, we feel that the mass loss may be inextricably linked to the dynamical excitation seen in the Kuiper Belt, which likely resulted from a process associated with the formation of the giant planets.

Formation theories for the giant planets divide (simplistically) into two classes: *direct collapse models*, where the local nebula quickly collapses into an almost full-mass gas giant, and *core instability models*, in which a solid central core formed by gravitational accretion subsequently accretes a gaseous envelope (see Wuchterl, Guillot, & Lissauer 2000 for a recent review). The timing and location of the formation of the giant planets (both relative to each other and relative to the terrestrial planets) is still debated (Kortenkamp & Wetherill 2000; Thommes, Duncan, & Levison 1999). Regardless, once the giants reach roughly their current masses, orbits initially confined between them become unstable due to the planetary gravitational perturbations, and almost all destabilize on timescales of 10^5–10^8 yr (Lecar & Franklin 1973; Gladman & Duncan 1990; Holman & Wisdom 1993; Holman 1997; Brunini & Melita 1998) The resultant planet-crossing orbits are rapidly ejected from the solar system, some going into the Oort cloud (Fernández 1978; Hahn & Malhotra 1999), some being inserted into the scattered disk (Torbett 1989; Duncan & Levison 1997), and others impacting the giant planets, resulting in a heavy-element enrichment in their envelopes (Guillot & Gladman 2000). Essentially the entire region between the giant planets was emptied on a timescale much shorter than the age of the solar system.

The Kuiper Belt is beyond the limits of the scattering action of the giant planets (on their current orbits). Some event, or events, after the accretional epoch produced the orbital structures, and these structures *require* some additional process that is more complicated than simple accretion and collisional erosion. Several models have been proposed, all of which have appealing facets, but no single process explains all the available facts.

Sweeping mean motion resonances.—Extending the realization of Fernández & Ip (1984), that angular momentum conservation caused Neptune and Uranus to migrate outward as the interplanetary planetesimal population was eliminated, Malhotra (1995) proposed that TNOs on originally nearly circular orbits could be trapped in Neptune's mean motion resonances as they swept past. This scenario is immensely appealing, as it provides a natural mechanism for the presence of the first known subcomponent of the Kuiper Belt—the high-e Plutinos—and predicts resonance trapping in the other mean motion resonances as well. The inclination distribution of *Plutinos* can be reproduced (Malhotra 1998; Gomes 2000). Hahn & Malhotra (1999) and Ida et al. (2000a) extended these ideas, demonstrating how sweeping operates under a variety of disk masses and migration timescales, and calculated relative trapping rates in the various resonances. A severe drawback is that resonance sweeping produces almost no inclination excitation beyond 42 AU. The sweeping process alone produces little mass depletion, because objects are either captured into the resonance (and thus protected) or "passed over and left on stable orbits with mild e. Finally, resonance sweeping produces almost no effect on orbits outside of the 2:1 resonance at 48 AU; if this were the only process operating, a cold TNO disk must be found outside this limit (Hahn 2000). The trapping process requires relatively adiabatic conditions, and so, if other large protoplanetary embryos even as small as the Moon are present in the disk, the resulting "jumps" in Neptune's migration during encounters with these objects produce very low capture efficiencies (Hahn & Malhotra 1999).

Planetary embryos.—Morbidelli & Valsecchi (1997) and Petit, Morbidelli, & Valsecchi (1999) developed a scenario in which massive giant-planet embryos (lunar- to Earth-sized or even larger) formed simultaneously with the giant planet cores are subsequently scattered onto orbits making repeated passes through the Kuiper Belt before being ejected from the system. The passing embryos are very effective at producing dynamical excitation in e and i, as well as mass depletion, but would have left very few objects in the 3:2 resonance. The details of the excitation structure and its radial extent depend on the orbital histories of the large bodies and are dominated by the largest embryo that lives an appreciable time. A single Earth-mass body surviving 100 Myr in the scattered disk would produce considerable velocity excitation ($e \sim i \sim 0.3$).

Resident planetary objects.—We propose here that the present TNO orbital structure could be the result of interaction with "planet-sized" ($D > 1000$ km) objects that have remained in the region outside of Neptune's current reach

($\sim$40 AU) for the age of the solar system. Such objects could result from gravitational interaction of scattered massive embryos, whose *mutual* close encounters place some of them on orbits that do not cross Neptune's, dynamically decoupling them from the planet and thus "stranding" some of them in the distant Kuiper Belt after the other massive bodies were eliminated by Neptune. Alternatively, a few lunar- or Mars-sized bodies (or even larger?) might have *formed* in the region outside 48 AU (say, 50–100 AU), some surviving for the age of the solar system; their mutual gravitational interaction is capable of giving them moderate eccentricities. The gravitational perturbations of such bodies (with surface escape speeds $\sim$2–5 km s^{-1}) is large enough to produce considerable excitation when integrated over the lifetime of the solar system, thus disrupting a "cold disk' outside 48 AU, with the details of the excitation dependent on the embryo's e and i. A Mars-sized TNO at 80 AU has $m_R \sim 19$ (for a 4% albedo), and so planetary bodies up to this size could have escaped detection in previous surveys. In particular, such resident bodies may be on highly inclined orbits (from the mutual scattering) which pass little time within 10° of the ecliptic, where previous surveys have concentrated. Even larger and brighter bodies would thus have remained undetected by the photographic surveys, if they are at present away from their nodal intersections with the ecliptic.

Temporary giant-planet passages.—Thommes et al. (1999) discussed a scenario in which the cores of Neptune and Uranus form between 5 and 10 AU; the greater mass density in this region allows them to form rapidly, avoiding the well-known problem (Hayashi, Nakazawa, & Nakagawa 1985) that accretion of their cores at their present distances may take much longer than the gas lifetime of the disk ($\sim 10^7$ yr). In this model Uranus and Neptune are scattered outward by Jupiter and Saturn, on Kuiper Belt–crossing orbits, before being circularized near their present distances by dynamical friction with a massive planetesimal disk. Another possibility is that *additional* cores, or even full-sized gas giants, were present and subsequently ejected, with the eccentricities of the remaining four planets being reduced either by dynamical friction or other dissipative processes (Levison, Lissauer, & Duncan 1998; Gladman 1998). The disadvantages of these models are that dynamical friction may require unreasonably large masses in the planetesimal component and that resonant trapping is relatively inefficient.

These models suggest another conceptual structure, that of the *fossilized scattered disk* (Thommes et al. 1999), an entity that would also appear to a lesser extent in the passing planetary embryo model. If Neptune, or any other massive object now removed, spent appreciable time (even $\gtrsim 10^5$ yr) transiting through the region outside 35 AU, it would scatter objects to high e, i, or both, with the largest pericenters near the aphelion of the massive body. The amplitude of the perturbation depends on the mass and orbit of the intruder and the duration of the crossing episode. After a massive perturber is removed or Neptune's eccentricity drops (decoupling it from the scattered region), the scattered structure left behind ("fossilized") becomes dynamically stable. The structure's extent depends on the aphelia of the massive scatterers, but could strongly deplete the region outside 48 AU. Evidence for this hypothesis would be the discovery of bodies with $q > 38$ AU (the limit of scattering perturbations that Neptune provides from its current orbit) with large e that are well separated from a "cold" (low e and i) Kuiper Belt component (see Gladman 2001).

Passing stars.—Ida, Larwood, & Burkert (2000b) propose an excitation hypothesis that works "from the outside in," in which the close passage or passages (perihelion $\sim$100–200 AU) of a star disturb TNO orbits. A single, or a few, stellar passage(s) can produce e- and/or i-perturbations comparable to the observed values beyond 42 AU, with the pericentric distance and passage angle as tunable parameters. This model then uses subsequent resonance sweeping to trap the resonant population and is thus constrained to only mildly perturb the region inside 40 AU. Potential problems are that the timescale to build the largest $\sim$1000 km TNOs may be longer than the 10^6–10^8 yr timescale of the young stellar encounters and that there is no mass depletion in the 30–50 AU region, which Ida et al. (2000b) ascribe to subsequent collisional processes. The stellar passage model is unique in producing an excitation with no outside edge (see also Fernández & Brunini 2000), whereas perturbations from other models discussed above would end at some heliocentric distance, allowing the existence of a dynamically "cold disk" sufficiently far from the Sun.

Disk evaporation.—This is a physically plausible process in which the outer portions of protoplanetary disks are evaporated via radiation from either the central star or a luminous nearby star (see Hollenbach, Yorke, & Johnstone 2000 for a review). Such "truncated disks" are seen in Orion on $\sim$50 AU scales; radiation has apparently evaporated all dust mass exterior to some limit. The fact that other evolved protoplanetary disks show dust distributions to large heliocentric distances (hundreds to thousands of AU) does not rule out this process as generic, because dust generated inside 50 AU might later be pushed outward by radiation pressure. Alternatively, bodies accreted *interior* to the evaporation limit might later be placed into a scattered disk; dust generated via collisions inside this component could be what is being observed (Trilling, Brown, & Rivkin 2000).

This concludes the framework within which our observational work is being carried out. Discrimination between present models will require a detailed understanding of the orbits of a very large number of TNOs (perhaps thousands). In many cases the region of heliocentric distances outside 50 AU is an evident lever arm for distinguishing between these theories, and it provided strong motivation for our deep imaging work dedicated to finding small, distant TNOs to examine the radial distribution of the trans-Neptunian population. We attempted to improve estimates of the luminosity function in order to examine the size distribution and mass of the belt. Finally, we wished to explore the inclination distribution of the belt as a diagnostic of the dynamical excitation; this last item will be explored in a separate paper (Kavelaars et al. 2001).

4. OBSERVATIONS

Our current observations continue in the theme of those described in our previous "pencil beam" surveys (Gladman & Kavelaars 1997; Gladman et al. 1998), concentrating on a single field each night to obtain maximum depth instead of areal coverage. Using the 3.6 m Canada-France-Hawaii Telescope (CFHT) and the ESO 8 m Very Large Telescope (VLT) UT1, we obtained deep R-band imaging of two ecliptic fields. The UT1 reached greater depth on a much smaller

TABLE 1

SUMMARY OF NEW PENCIL-BEAM SEARCHES FROM THIS WORK

Source[a]	UT Date	R.A. (J2000)	Decl. (J2000)	Time[b] (hr)	Filter	FWHM (arcsec)	Comment
CFHT/12k	1999 Feb 16	9 32 03	+17 24 27	5.167	R_{CFH}	0.7–0.9	Search
	1999 Feb 17	9 31 59	+17 24 27	5.333	V_{CFH}	0.9–1.4	Recovery
VLT/FORS1.....	1999 Jul 11	19 24 14	−20 58 45	5.160	R_{Bess}	0.4–0.7	Search
	1999 Jul 10	19 24 18	−20 58 45	6.360	R_{Bess}	0.6–1.1	Recovery

NOTE.—Units of right ascension are hours, minutes, and seconds, and units of declination are degrees, arcminutes, and arcseconds.

[a] Telescope/instrument combination.

[b] Total exposure time used for the pencil-beam study.

field. We discuss the data acquisition and preprocessing for these data sets separately.

4.1. *CFHT*

CFHT images were acquired on two nights in 1999 February under good conditions (see Table 1) using the prime-focus CFH-12K mosaic camera (Cuillandre et al. 2000) of 12 2K × 4K CCDs. At this date, only 10 of the 12 CCDs were science grade; one CCD suffered from a nonlinear sensitivity and another from substantial charge transfer problems. A plate scale of $\approx 0\farcs206$ pixel^{-1} means that the usable mosaic covered a nominal area of $35' \times 28'$. The known TNO 1997 CV_{29}, located in a sparse stellar field during the time of our observations, was used as a target to provide a fail-safe check of our recombination software; this object was easily located and measured (MPEC 1999-D07).

Single exposures were 8 minutes to avoid trailing losses; the fastest-moving objects at pericenter (Plutinos near 30 AU moving $\sim 4''$ hr^{-1}) suffer $\sim$0.1–0.3 mag of trailing loss Hainaut et al. 1994, but previous surveys (Jewitt et al. 1998) have shown that this is a small fraction of the total population; in any case, almost all high-e Plutinos are phase protected from being near pericenter in February as a consequence of the location of Neptune. Our best night produced 38 exposures of the target field; 35 were deemed of high enough quality to be included in the data analysis, yielding 16,800 s of integration. The sky brightness and image quality were reasonably constant through the night. Monitoring the photometry of bright stars in the field confirmed that the nights were photometric (Fig. 3). For non-moving point sources in $0\farcs8$ seeing at CFHT we expect this integration time to reach a limit of $R \sim 26$ at a signal-to-noise level of about 8, comparable to data from the Palomar 5 m obtained in our previous work (Gladman et al. 1998). During evening and morning twilight we obtained a long series of short exposures for removal of instrumental sensitivity patterns. Individual chips of the mosaic were reduced separately using the standard IRAF[2] CCDRED tools. The remaining sensitivity variations are less than $\sim$2%, and these small fluctuations are completely removed via our data recombination method. We observed Landolt standard field SA 98 (Landolt 1992) during short breaks in the pencil-beam observations. Calibration pointings were selected so that calibrator stars fell on each chip; because each mosaic CCD was processed separately, each had a separate photometric zero point determined to an accuracy of ± 0.03 mag.

4.2. *VLT*

Our VLT data were obtained during service observations in VLT queue-mode operations, using the FORS1 (Appenzeller et al. 1998) camera on UT1. That is, the observation request was defined by a set of parameters that was held in the service queue until observing conditions meeting that of our program (photometric sky with seeing better than $0\farcs8$) were met. During 7 hr portions of the nights of 1999 July 10 and 11, between 40 and 50 432 s R-band images were acquired of a $6\farcm7 \times 6\farcm7$ field. The seeing conditions were excellent and photometric conditions were very stable (Fig. 3). The data was processed by the service-mode pipeline, which removed most of the instrumental signature ($\sim$2%).

Because these observations were acquired just a few months after the beginning of science operations, the FORS1 zero point was still below its design specifications; we obtained 1 e^- s^{-1} for $m_R = 27.5$, significantly below the expected zero point of 28.0–28.1 (being reached as of 2000 March). Even though in dark conditions, the sky brightness of our images never dropped below $m_R = 20.5$ arcsec^{-2}, about 0.4–0.5 mag brighter than expected and also penalizing our final depth; the target field was taken by the observing queue in July, and thus the high stellar density at low Galactic latitude appears to pollute the sky background.

5. ANALYSIS

The CFHT and VLT images were analyzed in an identical fashion. The photometric zero point of each CCD was independently determined. An isolated bright star, free from cosmic rays on all exposures, was used to construct a point-spread function (PSF) for *each* exposure. Using these PSFs, artificial moving objects of random magnitudes were added to the images prior to further manipulation. Images were flux-equalized using the bright reference star and high-pass filtered to remove all large-scale gradients. They were then shifted and combined at rates of motion and directions consistent with outer solar system objects at opposition and examined visually to find the moving objects as described in G98. This "shift-and-add" technique results in a moving point source giving maximum signal-to-noise ratio when the direction and rate of motion of the recombination are most similar to the object's true motion. CB99 give an excellent discussion of the accuracy of this method for determining object rate, direction of motion, and magnitude; our

[2] IRAF is distributed by the National Optical Astronomy Observatories, which are operated by the Association of Universities for Research in Astronomy (AURA), Inc., under cooperative agreement with the National Science Foundation.

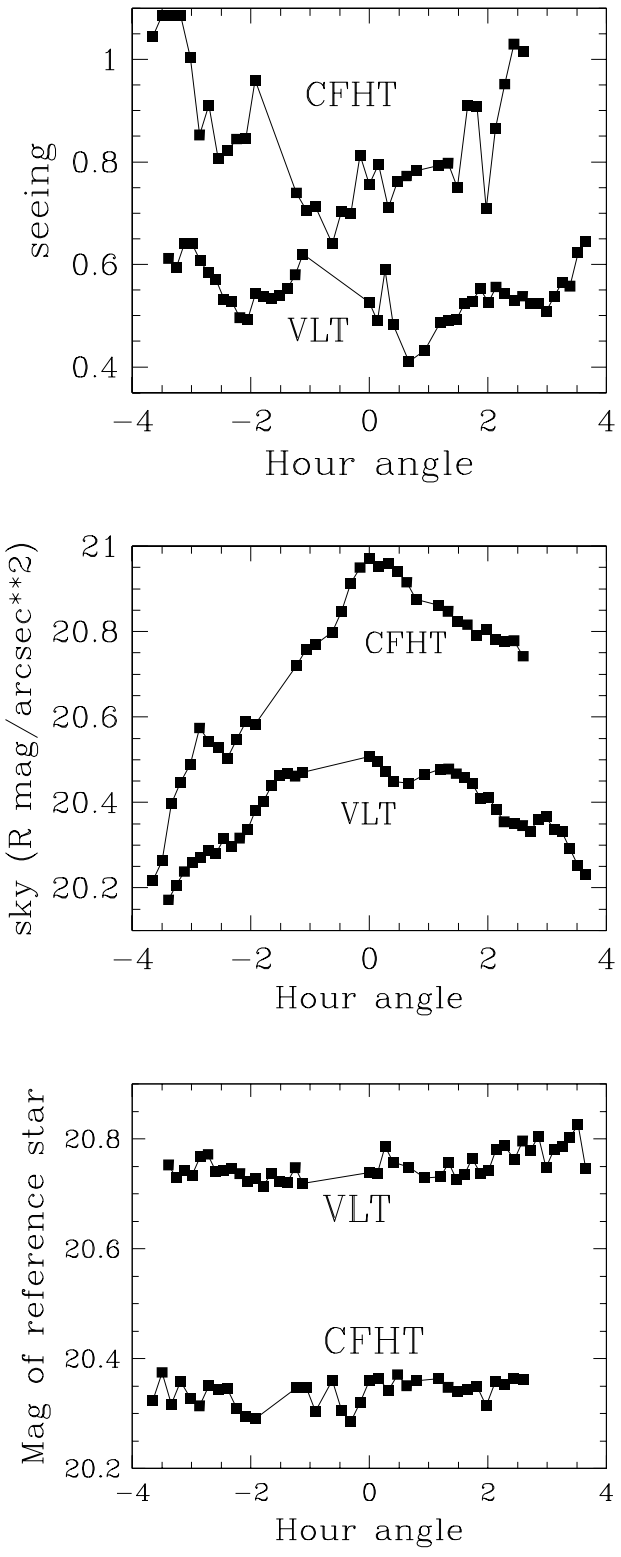

FIG. 3.—Summary of the observations on the two nights providing our two main search fields. The seeing shown is that of a single isolated reference star (evidently a different star for each telescope), whose photometric stability at the ± 0.05 mag level is shown at bottom. Sky brightness was confirmed on all the CFHT mosaic's chips; the feature near HA $= -3$ is real.

tests yield very similar results. Our tests showed that we are sensitive to objects moving within $\pm 5°$ of an assumed direction. Measured errors in rate and direction for identified objects are less important because our detection of all TNOs on two nights dramatically reduces this uncertainty.

The fake-object planting routine placed a random number of TNOs (100–140) into the frames at random positions, at random rates and directions, and at random magnitudes over a magnitude range (23.5–27.5 for CFHT, 24.0–28.5 for VLT), such that $\sim 70\%$ of all planted objects are brighter than our expected detection limit. With ~ 100 artificial objects on each CCD image, we are sensitive to both the magnitude incompleteness effects and the problems caused by stellar confusion and cosmetic flaws (assuming they cause problems at more than a non-negligible $\sim 1\%$ level). Planted objects had retrograde rates from $1''.3$ to $6''.4$ hr^{-1} and directions within 5° of the local ecliptic plane. Rates from $1''.2$ to $6''.6$ hr^{-1} were used for the search, corresponding to opposition distances from about 20 to over 100 AU. By recombining at three apparent directions on the sky, that of the ecliptic on the date of observation and $\pm 5°$ from it, we are sensitive to *all* orbital inclinations, because the intrinsic motion of the object is small compared with the retrograde rate; G98 incorrectly stated that sensitivity was only to inclinations less than 45°.

Object implantation was done by the computer and the information hidden in a file until after the search was done. It is important to search these data with the artificial objects implanted first so that any bias in the search procedure is the *same* for real objects as for the artificial ones. Three observers searched the entire rate range for each chip, but a given observer examined only one of the three angles relative to the ecliptic. Each searcher created a list of candidate TNOs, which were then compiled together, identifying all double detections (bright objects were usually found by all observers, while objects near the limit may be found only by the observer closest to the correct recombination angle). At this point the candidate list was compared with the implanted object list, generating an efficiency function for the implanted objects (see below) and a candidate list of a small number (zero to four per chip) of potentially real TNOs. These candidates were critically reexamined to determine their reality via further analysis. Real objects (average 1.7 per chip at CFHT) were usually evident and detected by multiple searchers; a few proposed objects (zero to two per chip) were rejected upon closer reexamination of the data (overlapping of two shifted stars was the most common, but easily detected, problem) with the benefit of the entire rate-angle grid around the TNO (see CB99 for an illustration). "Stage 2" verification of real objects consisted of recombining the nonplanted images *and* of combining the adjacent night at the known object rate to recover the TNO; success in both of these was necessary to be considered a true detection. The recovery nights (Table 1) were not searched for objects but only used for recovery verification. In fact, we had a zero "false detection" rate at the end of stage 1, in that no objects pursued in stage 2 turned out to not be real.

We did not "push" our search as deep into the noise as CB99; our searchers only accepted objects of which they were almost certain. The reanalysis, after the three searchers' results were combined, resulted in *only* real objects being followed to stage 2. Since this "bias" is present for the real and false objects, the detection efficiency we present is *accurate for this survey*, even if some real objects with low signal-to-noise ratio were eliminated. This will allow us to accurately "debias" our magnitude distribution. Our detection efficiency data are shown in Figure 4. The bright end of the function reaches effectively 100% efficiency as a result of the extremely low level of confusion

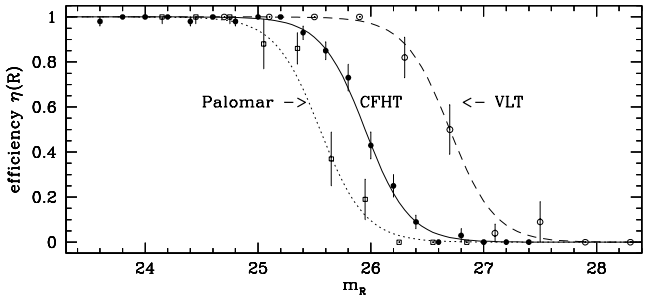

FIG. 4.—Efficiency functions for our main surveys, giving the fraction of artificially implanted objects found as a function of their apparent *R*-band magnitude. The fits shown are to eq. (2), with resulting parameters listed in Table 3. The CFHT data show small scatter because over 1000 fake TNOs were implanted over the entire mosaic. The Palomar data is that for the 1997 September survey.

in the median images we construct (Fig. 5). Bright objects can still be lost if they overlap with bad regions of the CCD, or pass in front of an extended bright galaxy or a very saturated star, but it is clear that this occurs for $\lesssim 1\%$ of the search area. CB99 correctly point out that the signal-to-noise ratio for objects near the noise limit is slightly higher in an average recombination than in a median. We decided to remain with the median because of the excellent rejection of very bright stationary objects (Fig. 5) and better cosmetics of the "median images" (see G98), which made them easier to search rapidly (924 median images were searched visually by our team in the process of this analysis).

5.1. *Detections*

The objects discovered at CFHT are listed in Table 2. No objects were found in the VLT data; considering the $m_R = 26.7$ depth of the VLT search, the null detection is consistent with the expected surface density given the field of view. The CFHT search's much larger area more than compensated for its somewhat shallower depth.

Only limited orbital information is available from a 24 hour arc. The observed angular rate gives a distance estimate accurate to $\sim 5\%$–10%; our detections range from about 30 to 60 AU, with 1999 DG_8 being the first object ever observed outside of 50 AU and still the most distant object ever observed in the solar system. The orbital node and i are well determined even for short arcs because the observations were on the ecliptic. In contrast, a and e are very assumption dependent, since a very large range of orbital parameters can give apparent rates at opposition matching those observed (see Bernstein & Khushalani 2000). It is important to realize that if a very inaccurate e is assigned, the heliocentric distance and potentially i provided by the incorrect orbit are forced away from their correct values; many lost high-i Plutinos may have been scattered objects whose large e produced the faster motion perpendicular to the ecliptic.

Most of these discoveries are so faint that recovery is extremely difficult. CFHT observations in 1999 March 23 by M. van Dalfsen, D. Hanes, and J. J. K. recovered 1999 DA, DB_8, DH_8, and DL_8. Observations by G. Bernstein et al. on 1999 May 10 recovered 1999 DA and DH_8. An attempt at CFHT by our team in 2000 March to recover all the objects failed in poor weather; only 1999 DA and DH_8 (the brightest two TNOs) were seen on one night (2000 March 30). Recovery observations in 2001 February from the VLT UT1 recovered 1999 DA and DH_8, producing 3 yr arcs.

The CFHT objects are at ecliptic longitudes where Plutinos would be preferentially at aphelion; only very large amplitude librators could be interior to 40 AU. We are thus suspicious of the Plutino orbits assigned to 1999 DA_8 and DD_8 on these grounds; in fact we have integrated 10 test

TABLE 2

TNOs DISCOVERED IN 1999 FROM THIS PENCIL-BEAM WORK (ORDERED BY INCREASING DISTANCE)

Name	m_R (error)	D (km)	Motion (arcsec hr^{-1})	r (AU)	i (deg)	a? (AU)	e?	Arc (days)
1999 DA_8	26.3 (0.5)	25	4.5	27.1	40	39?	0.3	1
1999 DD_8	25.8 (0.3)	55	3.5	37.8	5	39?	0.2	1
1999 DB_8	25.3 (0.3)	75	3.5	38.2	22	42.5	0.10	35
1999 DO_8	25.8 (0.3)	70	3.2	41.8	3	41.8	0.00	1
1999 DL_8	25.5 (0.2)	85	3.1	42.5	6	42.5	0.00	35
1999 DH_8	24.5 (0.2)	135	3.1	42.8	4.5	44.3	0.07	3 yr
1999 DM_8	25.6 (0.2)	80	3.1	42.9	4	42.9	0.00	1
1999 DF_8	26.5 (0.5)	55	3.0	44.2	3	44.2	0.00	1
1999 DN_8	25.8 (0.3)	80	3.0	44.3	3	44.3	0.00	1
1999 DQ_8	25.9 (0.3)	80	2.9	45.3	14	45.3	0.00	1
1999 DE_8	25.6 (0.2)	90	2.9	45.6	4	45.6	0.00	1
1999 DC_8	26.2 (0.4)	70	2.9	45.9	5	45.9	0.00	1
1999 DA	24.0 (0.1)	200	2.8	46.3	2.8	43.4	0.07	3 yr
1999 DZ_7	25.6 (0.3)	110	2.7	49.9	14	39?	0.3	1
1999 DR_8	25.3 (0.2)	130	2.7	50.6	8	46?	0.1	1
1999 DP_8	25.8 (0.3)	115	2.6	53.0	38	116?	0.70	1
1999 DG_8	25.6 (0.3)	165	2.3	61.0	40	82?	0.6	1

NOTE.—All objects were discovered on 1999 February 16 and reobserved on 1999 February 17. Diameters are computed assuming albedos of 0.04, have been rounded to the nearest multiple of 5 km, and are uncertain to factors of 2–3. The heliocentric distances r and inclinations i are much more reliable than the semimajor axes a and eccentricities e, since the latter quantities are assumption dependent for short arcs; especially uncertain a-e combinations are noted with a question mark. Orbits with $e = 0.00$ were forced to preliminary circular fits. Arc is the length of the observed arc, in days or years.

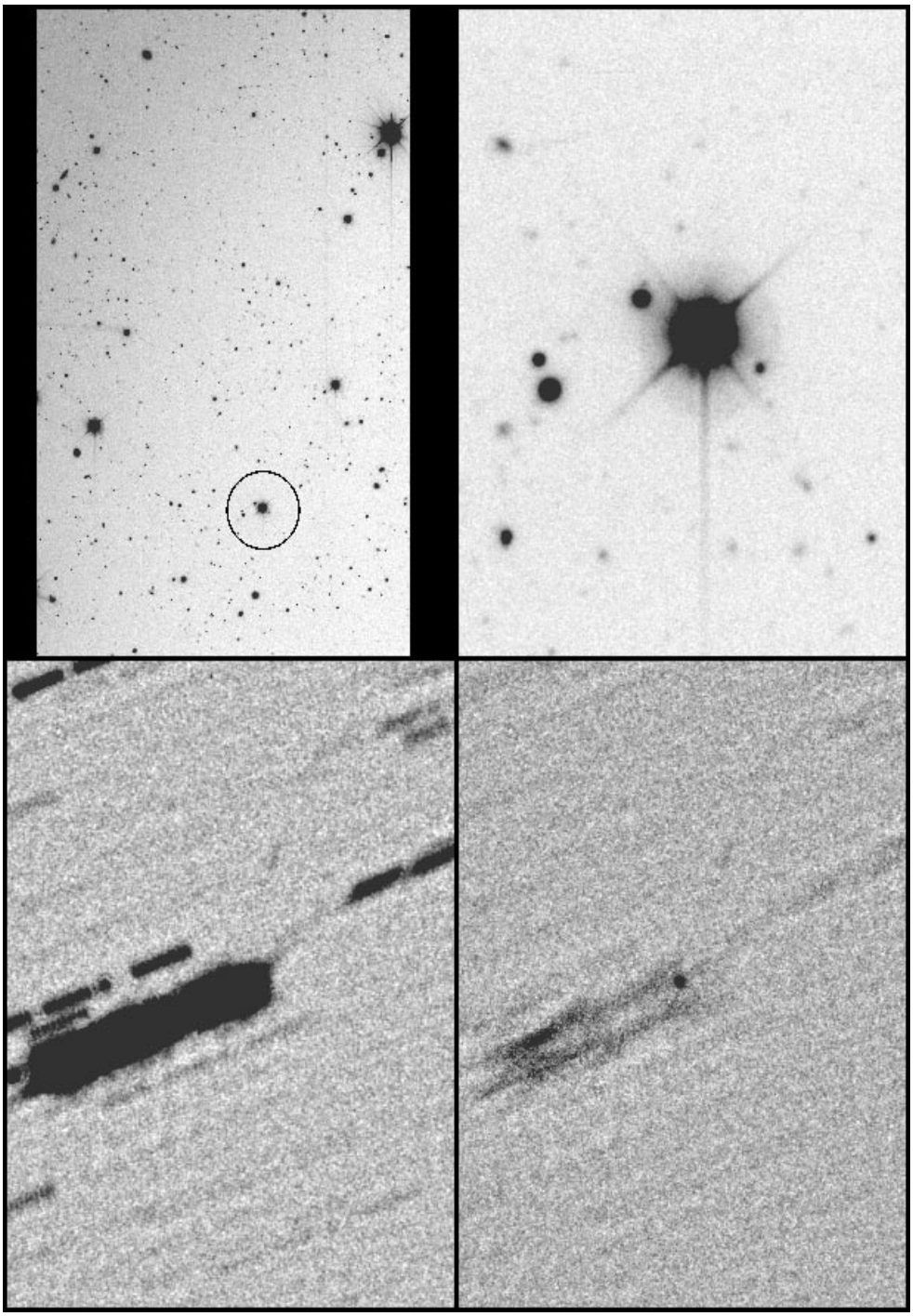

FIG. 5.—Illustration of how the pencil-beam technique reaches very high efficiency. The top left panel shows a segment of a 2K × 4K CFH 12K CCD frame, in which a 14th magnitude star (*top right*) is prominent. It can be seen that bright stars and galaxies cover a few percent of the full frame. The bottom left panel shows the result of an average of the shifted and recombined set (after scaling and filtering); the prominent stars from the top right panel are clearly visible as trails that have short breaks due to focus or calibrator exposures that interrupted the sequence. The bottom right panel shows the median image, which suddenly exposes a 24th magnitude TNO that began the sequence directly in front of the bright star. This dynamic range of more than 10 mag shows why we reach very close to 100% efficiency for all bright objects in the pencil-beam approach; only the brightest and most extended galaxies contaminate a sufficient number of the frames that the median does not eliminate them from the final analysis frames.

particles with or very near the MPC DA_8 orbit and found their orbits to be unstable on a timescale of less than 10 Myr. A Plutino orbit was also initially assigned to 1999 DB_8, but our 1999 March recovery eliminated the Plutino hypothesis. Because Plutinos are estimated to make up $\sim$10% of the population interior to 50 AU (Jewitt et al. 1998), it is possible that 1999 DZ_7 is a high-e Plutino near aphelion as assumed, but at $r = 50$ AU this requires forcing the highly eccentric and inclined orbit.

5.2. *Bayesian Analysis*

To revise our estimates of the Kuiper Belt's luminosity function we analyze the surveys available in the literature using a Bayesian method described in G98. Because of the

extreme importance of the correction for efficiency near the limit of the surveys, we only incorporated published surveys with detailed efficiency functions (Table 3). Efficiency curves for our surveys are well represented by functions of the form

$$\eta(R) = \frac{1}{2}\left[1 - \tanh\left(\frac{R - R_{50}}{W}\right)\right] \quad (2)$$

and functions for other surveys are given in Table 3. Using object magnitudes, the survey's areal coverage and efficiency function, and the methods described in G98, we estimate the parameters of a cumulative luminosity function of the form

$$\Sigma(m_R < R) = 10^{\alpha(R - R_0)}, \quad (3)$$

where Σ is the number of TNOs with magnitudes brighter than R per square degree. R_0 indicates the magnitude where 1 TNO deg^{-2} is reached *in the ecliptic*; because the surface density falls off in a poorly determined fashion at higher ecliptic latitudes, we use only surveys which are within a few degrees of the ecliptic. Our parameter estimates are shown in Figure 6. Adding our new detections and the survey of CB99 has improved the confidence in the best-fit parameters $(\alpha, R_0) = (0.69, 23.5)$. Although CB99 quote a 50% detection limit of $R = 27.5$, they reject all candidates fainter than $R = 27.0$; thus we assign this survey a 50% limit of $R = 27.0$ but smooth the sharp cutoff by the estimated photometric uncertainty of 0.25 mag (CB99). Our parameter estimates are dominated (for obvious reasons) by the abundant objects in our 1999 February CFHT pencil-beam and the JLT98 survey; fitting only those two data sets yields $(\alpha, R_0) = (0.69, 23.4)$, but with larger uncertainties.

We have not incorporated the Keck survey of Luu & Jewitt (1998, hereafter LJ98), largely because a detailed efficiency function for this survey is unpublished. They conclude $\Sigma(<26.1) = 31^{+12}_{-14}$ deg^{-2}. Debiasing our 14 direct detections with $m_R < 26.1$ with our efficiency function yields 63 TNOs deg^{-2}, $\simeq 3\ \sigma$ higher than the LJ98 estimate (accepting their errors). Interpretation of the LJ98 survey is also difficult because, even though observed at opposition (D. Jewitt 2000, private communication), three of the detected objects (K3, K13, and KUD) have declination motions $\geq 2''.4$ hr^{-1}. Orbital computations by B. G. and independently by B. G. Marsden (2000, private communication) show that such motions are physically impossible for bound solar system objects at the proposed trans-Neptunian distances. Without more detailed knowledge of this survey, we are unable to resolve these discrepancies.

With misgivings, we present a binned representation of sky density estimates (Fig. 7). This representation of the data can be misleading, because (1) sparse data cause the binning to affect the plot, and thus the fits made to points placed upon it (especially important when efficiency corrections are performed at the *centers* of large bins); (2) the cumulative nature of the plot means the errors are correlated; and (3) upper limits and magnitude errors of individual TNOs are difficult to incorporate. Many workers plot Σ-estimates at the bin centers (even though the function is cumulative and thus Σ-estimates should be at the faint edge of the bins) and then use least-squares fits to the positive detections only. CB99 used a "running" Σ estimate (their eq. [3]) that avoids binning and thus incorporates the magnitude distribution and efficiency data in a less model-dependent way, but this estimate cannot account for surveys reporting only upper limits. Our analysis avoids all these problems.

In both LJ98 and CB99 a least-squares method is used, which is formally inapplicable to the type of data being considered, and at the very least the *uncertainties* in the parameter estimates (for α and R_0) are incorrect because the data do not satisfy the assumptions of a least-squares (modified minimum χ^2) approach of having uncorrelated Gaussian errors. We thus have no rigorous way of estimating the significance of disagreement between our best estimates and those of LJ98 and CB99 (Fig. 6*d*); while their best

TABLE 3

SUMMARY OF AVAILABLE SURVEYS WITH EFFICIENCY FUNCTIONS, USED IN OUR BAYESIAN ANALYSIS

Source	Ref.[a]	Ω (deg^2)	R_{50}	W	Magnitudes of Detected Objects, m_R (error)
VLT	G00	0.012	26.7	0.4	None
CFH/12k	G00	0.31	25.93	0.39	24.0 (0.1), 24.5 (0.2), 25.3 (0.2), 25.3 (0.3), 25.5 (0.2), 25.6 (0.2), 25.6 (0.2), 25.6 (0.3), 25.6 (0.3), 25.8 (0.3), 25.8 (0.3), 25.8 (0.3), 25.8 (0.3), 25.9 (0.3) 26.2 (0.4), 26.3 (0.5), 26.5 (0.5)
KECK/LRIS	CB99	0.010	27.0	0.25[b]	25.1 (0.4), 26.8 (0.4)
CFH/UH8k	JLT98	51.5	23.4[c]	1.0[c]	20.60 (0.2), 21.00 (0.2), 21.06 (0.2), 21.37 (0.2), 21.84 (0.2), 22.28 (0.2), 22.43 (0.3), 22.58 (0.3), 22.65 (0.2), 22.78 (0.2), 23.0 (0.2), 23.0 (0.2), 23.1 (0.3)
CFH/UH8k	G98	0.35	24.6	0.5	23.7 (0.2)
Palomar	G98	0.049	25.6	.38	22.95 (0.03), 24.0 (0.1), 25.6 (0.3), 25.8 (0.3)
Palomar	G98	0.075	25.0	0.5[d]	None
WHT	ITZ95	0.70	23.5	0.4[d]	22.4 (0.1), 22.9 (0.1), 22.9 (0.1), 23.3 (0.1)
HST	C95	0.002	28.1	0.6	See G98 for discussion
USNO 40 inch (1 m)	LD90	4.88	22.0	0.5[d]	None
UH 2.2 m	LJ98	.338	24.0	0.5[d]	None
Schmidt	LJ98	297.	20.0	0.5[d]	None

NOTE.—For each survey we indicate the survey parameters used, and the reference for further information on that survey.

[a] "G00" indicates this work.

[b] R-band uncertainties include a ± 0.3 mag uncertainty in the color conversion. See text for comments on R_{50} and W.

[c] Efficiency function of JLT98 is not of the form of eq. (2), but their functional form is not given. We fitted by eye a relation that duplicates their efficiency function to high precision. R-band uncertainties include a ± 0.2 mag uncertainty in the color conversion due to the use of the VR filter.

[d] Efficiency function taken to be linear decay from 100% to 0% from $R_{50} - W$ to $R_{50} + W$.

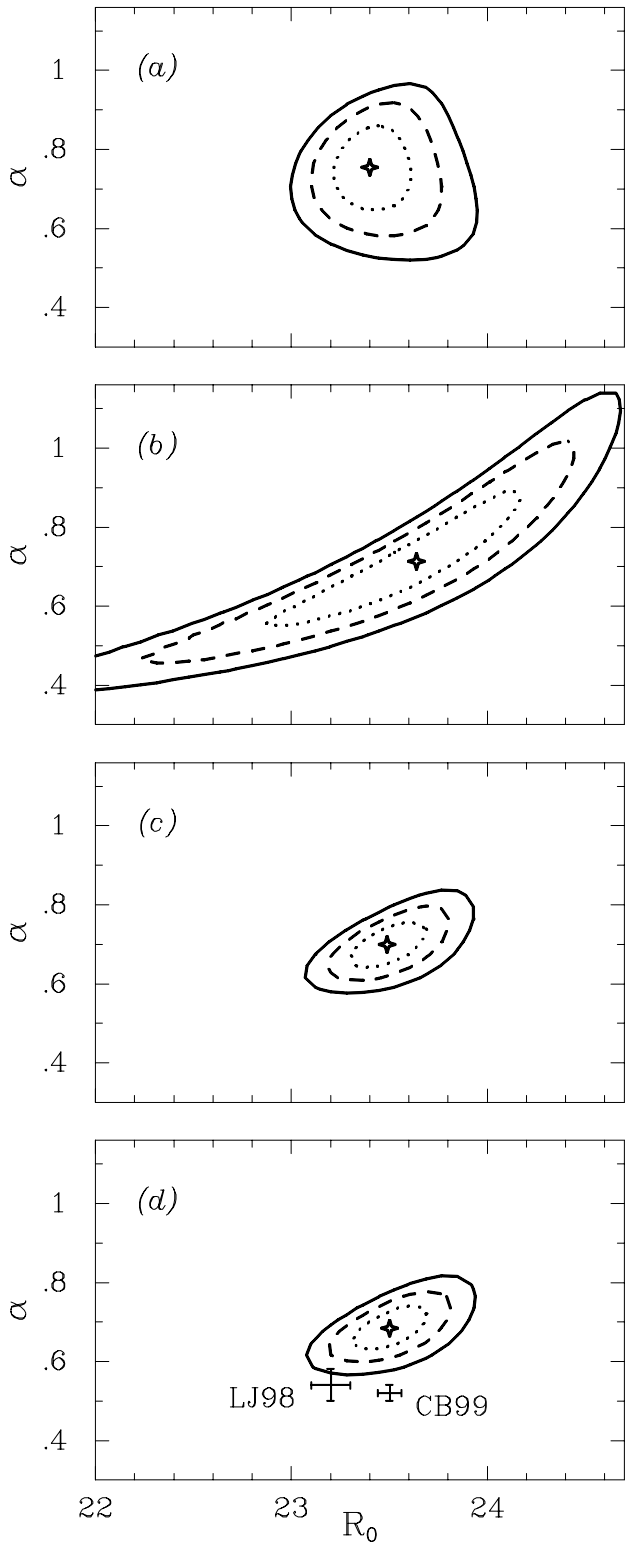

FIG. 6.—Estimates for the luminosity function's slope α and logarithmic zero point R_0. Contours show boundaries of 68.3%, 95.4%, and 99.7% credible regions. The point is the mode. (*a*) Previous result of G98. (*b*) Using only our pencil-beam data reported in G98 and this work. (*c*) All surveys in Table 3 *except* the VLT pencil-beam. (*d*) All surveys in Table 3. This last panel also shows the best estimates from LJ98 and CB99 with their given uncertainties (see text).

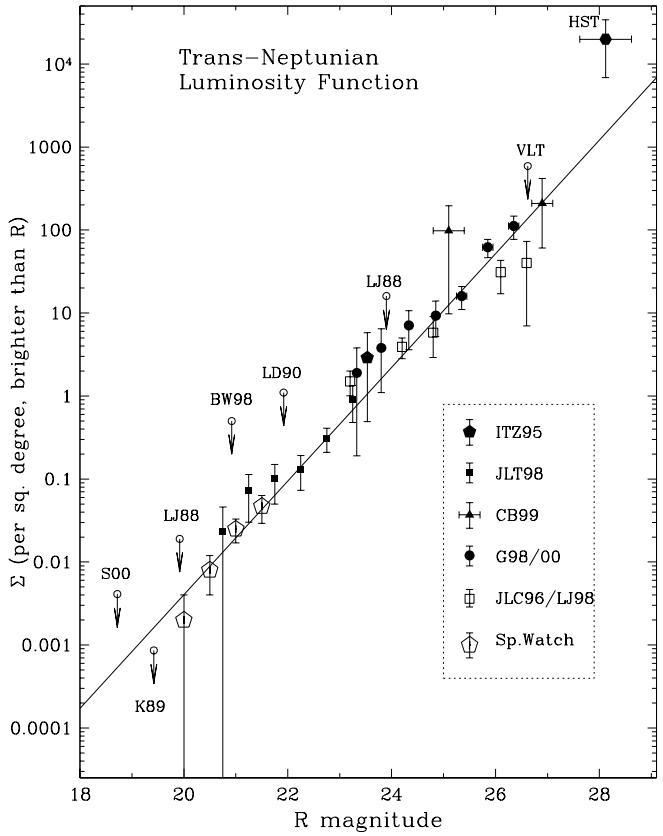

FIG. 7.—Representation of the cumulative luminosity function, showing various sky density estimates in the literature. This figure must be interpreted with extreme caution (see text). Filled symbols represent the surveys used in our analysis. The upper limits are 3 σ representations at the stated 50% limit of the survey; only the VLT, LJ98, Levison & Duncan 1990, hereafter LD90, and LJ98 upper limits were used in our analysis. The surveys BW98 (Brown & Webster 1998), K89 (Kowal 1989), S00 (Sheppard et al. 2000), and Spacewatch (Larsen et al. 2001) are shown for reference but not incorporated. The solid line shows the most probable distribution.

estimates are outside our 99.7% confidence limit, the least-squares derived error estimates are likely underestimated. Although all three analyses use somewhat overlapping sets of data, these sets are not identical; obviously, our new data were not present in their fits, and the LJ98 Keck survey is not present in our data analysis. When CB99 omitted the LJ98 survey (their Fig. 7*b*), their best fit was $(\alpha, R_0) \sim (0.66, 23.4)$, which is extremely close to our best estimate.

At the time of revision, we became aware of the bright, wide surveys of Sheppard et al. (2000) and Larsen et al. (2001). We have not attempted to incorporate their surveys into our analysis (although their small number of detections at bright magnitudes favors a steeper luminosity function), because these surveys have significant fractions of their search areas off of the ecliptic (this effect is less severe for the Spacewatch survey). The correction for the falloff of TNO density with ecliptic latitude (see, e.g., Jewitt et al. 1996; Elliot et al. 2000; Kavelaars et al. 2001) is uncertain and will require additional modeling.

6. SIZE DISTRIBUTION AND MASS OF THE BELT

The observed luminosity function can be used to estimate the TNO size distribution and mass of the disk, under a few assumptions. Suppose that the joint diameter–heliocentric distance distribution can be factorized (i.e., the size distribu-

tion is independent of the heliocentric distance) and that both are representable as power laws. The differential number of TNOs at distance r with diameter D is expressed as

$$n(r, D)dr\,dD = Ar^{-c}D^{-q}\,dr\,dD\,, \tag{4}$$

with q the differential size index and c the radial power-law index. The formal expressions derived below assume that $c \neq 1$, $q \neq 1$, and $2q + c \neq 3$ although all the physical quantities are well behaved at these points (with dependencies becoming logarithmic). Write the brightness scaling at opposition (eq. [1]) for TNOs with 4% albedos as

$$m_R = C + 2.5 \log r^4 D^{-2}\,, \tag{5}$$

where $C \simeq 18.8$. Restricting consideration to a range in heliocentric distances $r_{\min} < r < r_{\max}$, one obtains

$$n(m_R) = A\,\frac{\ln 10}{5}\,\frac{r_{\max}^{3-2q-c} - r_{\min}^{3-2q-c}}{3-2q-c}\,10^{(1-q)(C-m_R)/5}\,. \tag{6}$$

This can be integrated to give a *cumulative* luminosity distribution,

$$N(m_R < R) = \frac{A}{q-1}\,\frac{r_{\max}^{3-2q-c} - r_{\min}^{3-2q-c}}{3-2q-c}\,10^{(1-q)(C-m_R)/5}\,, \tag{7}$$

over the sky area of interest. The observed cumulative surface density (eq. [3]) then determines the normalization constant A because

$$N(m_R < R) = S\Sigma(m_R < R)\,, \tag{8}$$

where S is the area of sky studied. This establishes the relations

$$A = 5S\alpha 10^{\alpha(C-R_0)}\,\frac{3-2q-c}{r_{\max}^{3-2q-c} - r_{\min}^{3-2q-c}}\,, \tag{9}$$

$$\alpha = (q-1)/5\,. \tag{10}$$

Thus, the slope α and zero point R_0 of the cumulative luminosity function, with estimates of S and c, determine the total number of bodies in the interval $(r_{\min}, r_{\max})$ brighter than R, where R_0 must be estimated with only those objects inside the heliocentric distance interval of interest.

The index $q = 5\alpha + 1$ of the differential size distribution is seen to depend uniquely on the slope of the luminosity function (see Irwin, Tremaine, & Żytkow 1995 and CB99, although our derivation is more general in eliminating the approximation of constant distance for all TNOs). CB99 give an excellent discussion of the implications of various size distributions. For $\alpha > 0.6$ the mass of the total population is dominated by the smallest bodies; CB99 point out that such a steep slope would violate the mass constraint of $\sim 1\ M_\oplus$ inside 50 AU. This is correct *if* the steep distribution continues down to small TNOs (CB99 show that the mass constraint is violated if steep slopes continue down to ~ 1 km bodies), but there are very good reasons to believe that the size distribution will flatten out well above such small sizes. Davis & Farinella (1997) and Stern & Colwell (1997b) independently showed that objects with $D \gtrsim 50$ km have not had their size distribution modified by collisional processes over the age of the solar system. Thus, the size distribution of TNOs larger than this size can be taken as a signature of the accretional process. But objects *smaller* than about 50 km will have modified toward a Dohnanyi-like $q = 3.5$ index (Dohnanyi 1969), and so most of the mass of the belt would be concentrated around this turnover point. In fact, since a $D = 50$ km TNO at 35 AU has an apparent magnitude of $m_R \simeq 25.9$ (eq. [1]), surveys have not yet extended appreciably past the roll-over point.

What would be the observational signature of reaching this point? Imagine that the belt consists of the single power-law size distribution, but at each distance r the number of TNOs per square degree is normalized by some multiplicative factor $f(r)$ (related to the surface number density at that distance). As long as one does not pass the upper or lower diameter limits of the power law, at each distance the observer sees a luminosity function of the same slope; convolving all distances together gives a luminosity function with again this same slope. As one looks to fainter magnitudes m_R, this behavior could break down in two ways. (1) At great distances m_R corresponds to bodies larger than the maximum diameter in the distribution, and (2) objects at the roll-over diameter discussed above become detectable at the *inner* edge of the distribution. Neither possibility is likely to have occurred within the bounds of current surveys. The largest bodies presently observed out to 65 AU have diameters of 500–800 km, and there is no reason to expect that the largest objects have yet been found. A $D = 1000$ km body would be visible in our pencil-beam surveys (limit of $m_R \sim 26$) out well past 200 AU, so there is no reason to expect that observations have hit the upper diameter limit unless a dramatic maximum size limit suddenly occurs outside 48 AU (JLT98). The observational signature of reaching the roll-over diameter at the *inner* edge of the Kuiper Belt is that the luminosity function will flatten out since the closer annuli stop contributing as large a fractional increase in objects per magnitude interval. For mildly eccentric ($e = 0.2$) Plutinos near their perihelia at 32 AU, a limiting magnitude of $m_R = 25.9$ corresponds to $D = 40$ km and is just beginning to sample the sizes where collisional models predict the roll over to be. We do not believe that current surveys can reliably detect the roll-over effect, which will probably require tens of detections at the $D = 20$ km level into the classical belt (magnitude levels of 28–28.5). This will require a large-field mosaic camera on an 8 m class telescope, or a space-based telescope capable of directly imaging these moving objects without pencil-beam techniques (*Next Generation Space Telescope*). The sky density estimated by the *Hubble Space Telescope* (*HST*) pencil beam (Cochran et al. 1995, hereafter C95) would seem to imply a roll-over diameter of less than 50 km; our analysis in G98 showed that their statistical "on/off" detection was consistent with a null detection at the 2 σ level, and so another survey to this magnitude level needs to be performed.

Our results indicate that the differential size index in the observed region is $q \simeq 4.4 \pm 0.3$ (approximate because α and R_0 define a joint two-dimensional parameter uncertainty region). This size index is marginally steeper (although consistent within the errors) than the $q_0 = q - 1 = 3$ cumulative index rapidly approached by the accretional simulations of Kenyon & Luu (1999); their models then constrain planetesimal building to have proceeded in a cold environment for at least ~ 20 Myr but provide no upper limit. Davis et al. (1999) appear to require ~ 1 Gyr of accretion to approach this size index, which seems uncomfortably long in the context of the sculpting models discussed earlier.

Because the size distribution must eventually roll over, we can estimate the mass of the disk even though $q > 4$ in the observed region. We approximate the size distribution by a power law with index $q > 4$ for diameters down to the "knee" D_k in the size distribution at the roll-over point, and then with a Dohnanyi (1969) $q = 3.5$ law for all smaller sizes. In reality the size distribution should show "waves" below the knee (caused by the upper and lower cutoffs in an otherwise steady state distribution) similar to that in the asteroid belt (see, e.g., Davis & Farinella 1997); this will not dramatically affect the result, because we now show that the mass below the knee is minor compared with that above. Integrating equation (7) from infinity to the knee gives the population N_1 of bodies larger than D_k:

$$N_1(D > D_k) = \frac{A(r_{\max}^{1-c} - r_{\min}^{1-c})}{(1-c)(q-1)} D_k^{1-q} . \quad (11)$$

Since this is a cumulative distribution, it serves as a starting point on which to "anchor" the number distribution smaller than D_k down to some size D_0

$$N_2(D > D_0; D_0 < D_k) = \frac{A(r_{\max}^{1-c} - r_{\min}^{1-c})}{(1-c)(q-1)} D_k^{3.5-q} D_0^{-2.5} . \quad (12)$$

This diverges as $D_0 \to 0$, but the total mass M does not; the latter can straightforwardly be computed as

$$M = \rho \frac{\pi}{6} S\alpha 10^{\alpha(C-R_0)} \frac{(3-2q-c)(r_{\max}^{1-c} - r_{\min}^{1-c})}{(1-c)(r_{\max}^{3-2q-c} - r_{\min}^{3-2q-c})} \times \left[\frac{1}{q-4} + \frac{2}{2.5(q-1)}\right] D_k^{4-q} , \quad (13)$$

where a constant TNO mass density ρ is assumed, and on the condition that $q > 4$ (the mass above D_k diverges if not, and these expressions must be reexpressed in terms of the maximum size in the distribution). The two terms in equation (13) express the relative contributions to the mass from above and below D_k; the large bodies always dominate when $q > 4$ and "most" of the mass is in the order of magnitude in size just above the knee (a fraction of $1–10^{4-q}$, about 50% for $q = 4.3$). Note the "spin-off" benefit that if $q > 4$ above the knee, the mass estimate is robust, whereas if $q < 4$ the total mass is unknown until the largest objects are found (in which reside most of the mass).

Over the 30–65 AU distance range spanned by our observations, we use our best estimate of α and R_0 to estimate a total disk mass as function of D_k (Fig. 8). To a factor of 2, the disk mass estimate is insensitive to plausible variations in the radial number density or in D_k as long as the latter is over 3 km. Since literature estimates of M are often quoted for the 30–50 AU disk, Figure 8 also shows this calculation; care has been taken to eliminate TNOs outside 50 AU from the luminosity function (essentially changing R_0). The estimated mass of 0.04–0.1 $M_\oplus$ for the 30–50 AU belt compares well with previous observational estimates (JLT98; CB99); our analysis avoids uncertainties involved in modeling the orbital distribution, although we have mild model dependence in the parameter c. This estimate measures only the mass *currently* in the $(r_{\min}, r_{\max})$ range; the mass of the "scattered disk" (for example) is mostly distant and thus not contained in this estimate. Duncan & Levison (1997) calculate a radial power law for the scattered disk which could be included in refining this analysis. Trujillo et al. (2000) estimate a total scattered-disk mass, but only for those objects in the restricted perihelion range of 34–36 AU; given the models discussed in § 3, the real distribution could be much more extended and the scattered component correspondingly much more massive. Hahn & Brown (1999) pointed out that the inner edge of the Kuiper Belt may be dynamically "eroded' so that the surface density probably initially rises with distance.

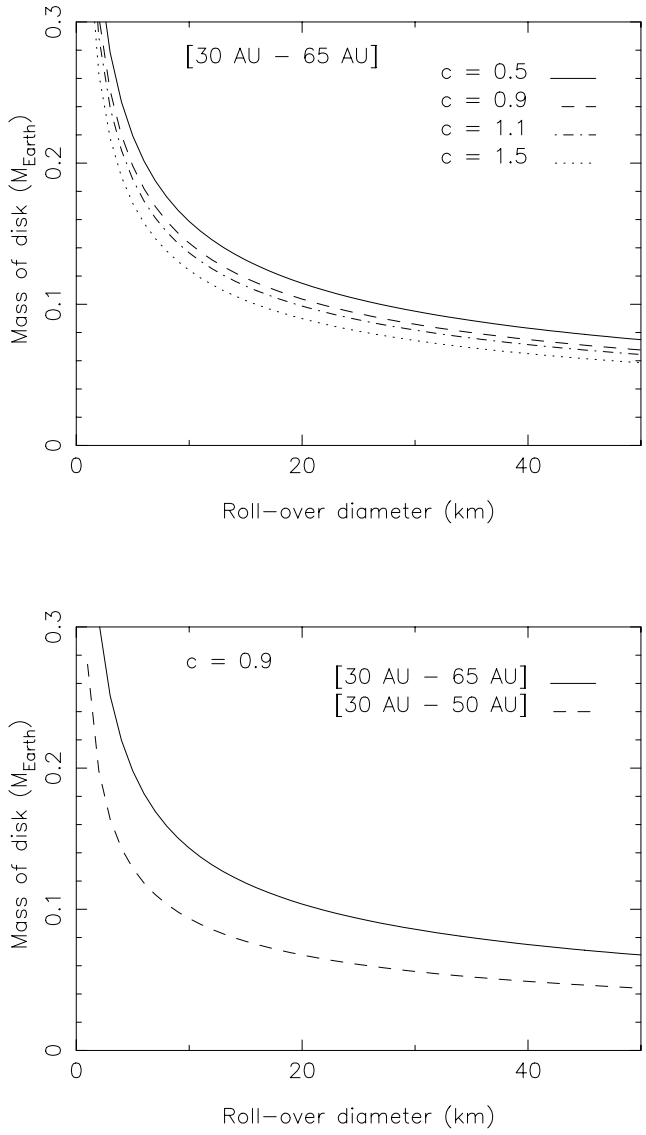

FIG. 8.—Mass of the disk as a function of the roll-over diameter D_k. *Top*: Disk mass for various radial power-law indices c, showing that the mass of the disk is only weakly dependent on physically reasonable ranges in this index. The total disk mass is not a strong function of D_k until D_k drops below 3 km. *Bottom*: Restricting the heliocentric annulus to 30–50 AU causes only an order-unity correction in the mass estimate.

7. CENTAURS

We have detected zero or one object inside 30 AU, depending on what orbit 1999 DA_8 is actually on (its heliocentric distance could even be larger than 30 AU given the

uncertainties). Jewitt et al. (1996) estimate 0.5 Centaurs per square degree at $m_R = 24.0$. Estimating the sky density at $m_R = 26$ with luminosity function slopes of $\alpha = 0.52$–0.7 yields 11–25 Centaurs deg^{-2}, predicting three to eight Centaurs in our fields. But this neglects inefficiency at the faint end and the fact that the rate range used for our pencil beam recombinations is insensitive to Centaurs inside Uranus. The fraction of Centaurs that are between 5 and 20 AU versus those between 20 and 30 AU is model dependent; Irwin et al. (1995) and Duncan & Levison (1997) provide estimates. Given the detection bias toward the closest objects (most of the known Centaurs are inside 20 AU), we feel that modeling zero to one detection is not merited (see Sheppard et al. 2000 for recent estimates).

8. THE REGION OUTSIDE 48 AU

The adoption of provisional circular orbits for the TNOs discovered with $r = 40$–47 AU (Table 2) has been standard practice, as has the common adoption of perihelic Plutino provisional orbits for objects found interior to 40 AU. However, up to the date of writing the Minor Planet Center has always assigned aphelic or highly eccentric orbits to TNOs discovered exterior to the 2:1 resonance. The placement of 1999 DR_8 at aphelion of an $a = 46$ AU orbit is entirely arbitrary. The hypothesis of "scattered' orbits of 1999 DP_8 and 1999 DG_8 is reasonable given their large declination motion, which indicates a significant inclination, but the (a, e) combination that is compatible with the observations is very large (cf. Bernstein & Khushalani 2000). For an object with nonnegligible motion perpendicular to the ecliptic, the adoption of a high-e orbit reduces i. The faster motion near pericenter at high e produces an apparently *faster* motion perpendicular to the ecliptic; if the orbit were really of lower e, the inclination would rise. A similar effect also occurs for heliocentric distance (even for $i = 0°$ orbits) because of the faster motion at pericenter; a low-e orbit must be farther from Earth to produce a given angular retrograde rate.

These uncertainties are especially important for understanding the region at or outside 48 AU, because here assumptions dominate the osculating elements. During our observing work we have attempted to understand the orbital bias by recovering as many of the distant TNOs as possible. Two examples will help characterize the level of uncertainty.

The TNO 1999 CZ_{118} was found by D. Jewitt, C. Trujillo, & J. X. Luu (MPEC 1999-D28) and assigned a provisional orbit, based on observations in 1999 February and May, of $(a, e, i, M, \omega) = (44.7, 0.094, 39°, 180°, 360°)$; that is, at the 49 AU aphelion of an eccentric classical belt orbit. A. M. and J. J. K. recovered the object in early 2000 January at CFHT (MPEC 2000-A40) very far (25′) from its predicted position; this recovery, with additional observation by Kavelaars et al. on 2000 March 29, caused the orbit to be revised to $(a, e, i, M, \omega) = (111, 0.657, 28°, 351°, 235°)$, that is, at 45.5 AU, just before pericenter in a much larger scattered orbit.

The TNO 2000 CR_{105} was discovered by R. L. Millis et al. (MPEC 2000-F07) and given a provisional $(a, e, i, M, \omega) = (81.8, 0.586, 31°, 331°, 99°)$ based on a 3 week arc, corresponding to $r = 55.4$ AU. This initial orbit was doubtlessly chosen to be "similar" to the orbit of 1996 TL_{66} (Luu & Jewitt 1998). Our 2000 March 28 and 29 recovery observations only 4 weeks later showed the object to be already noticeably off the ephemeris, and a strong orbital revision to $(a, e, i, M, \omega) = (675, 0.940, 23°, 0.°7, 310°)$ resulted (MPEC 2000-F43), corresponding to $r = 51.5$ AU. As this paper goes to press we have recently shown that $r = 53$ AU and $q = 44$ AU, with a uniquely large pericenter for a large-a TNO (Gladman et al. 2001).

Because of these extreme uncertainties, we will base our discussion on two better determined parameters: Figure 9 shows the heliocentric distances and absolute magnitudes for all objects in the MPC database (2000 July 8). Up to the end of 1998, no objects with heliocentric distances outside 48 AU had been detected, leading previous analyses to suggest that the TNO distribution was somehow truncated at or near this distance (see § 2).

1999 CZ_{118} appeared to be the first TNO discovery beyond 48 AU (noted by B. G. Marsden in MPEC 1999-D28), but recovery (discussed above) pushed it sunward. Of our four 1999 February detections with $r > 48$ AU (Table 2) the assumed aphelic orbits for 1999 DZ_7 and 1999 DR_8 mean they could be closer than 48 AU if a is much larger than assumed. Objects 1999 DP_8 and DG_8 seem firmly in the $r > 48$ AU regime, since they are already on large-a orbits near perihelion.

Comparisons between the number of expected and observed "distant" TNOs (i.e., further than the 2:1

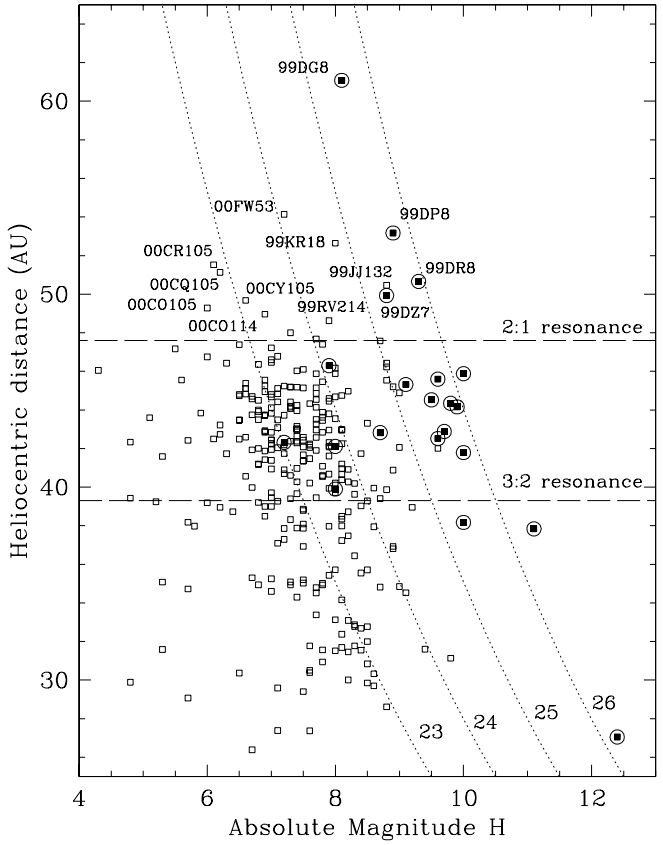

FIG. 9.—Distribution of distances and absolute magnitudes for cataloged TNOs, which are reasonably well determined even for objects with 24 hr arcs (±5%–10% in distance and ±0.5 mag). Curves of constant apparent R-band magnitude are marked. Objects discovered during our *pencil-beam* work (including G98) are solid and circled, and objects outside the distance of the 2:1 resonance are individually named, for reference. Objects 1999 KR_{18} and JJ_{132} were discovered by Allen et al. (2001) using pencil-beam techniques.

resonance) are now abundant in the literature. Essentially, the parameters that determine what fraction of the observed TNO population should be distant are (1) the radial distribution of TNOs, (2) the size distribution and its form (effectively, the luminosity function), and (3) the potentially varying dispersion perpendicular to the ecliptic of the Kuiper Belt's subpopulations. From analytical estimates using radial power laws or from Monte Carlo modeling, estimates for the fraction f of distant TNOs range from 40% to 50% (Dones 1997; Jewitt et al. 1998) for shallow luminosity functions, to figures more like $\sim 5\%$–10% for steeper slopes (G98; CB99; Hahn & Brown 1999). G98 predicted that a $30' \times 30'$ pencil beam to $m_R \gtrsim 26$ would establish f; our February CFHT survey in fact detected four of 17 TNOs outside 48 AU. More completely, four of the 22 TNOs discovered from our pencil-beam work since 1996 fall in this class—a fraction of $f = 18\%$. This surprises us somewhat, as we previously argued (G98) that under power-law assumptions for cases 1 and 2 above, the fraction of distant TNOs is *independent* of magnitude limit. As of the end of the summer of 1999, *only* pencil-beam surveys had found distant objects. Deep work by Allen et al. (2001) found three distant of 24 TNOs discovered ($f = 13\%$). Our interpretation in summer 1999 was that the "roll over" in the size distribution discussed had been reached. Jewitt et al. (1998) modeled their bright, wide surveys and concluded that there was no loss of sensitivity for distant objects, and thus fewer than one in the more than 100 TNOs discovered were distant. If this $f \lesssim 1\%$ was truly the fraction of distant objects, then the probability of us finding four is negligible ($<0.15\%$). But in early 2000, Millis et al. discovered five (of ~ 57) TNOs in their bright, wide survey to be distant, and Jewitt et al. have reported 1999 RV_{214} and 2000 FW_{53}. The ESO group (Delsanti et al. 1999; O. Hainaut 2000, private communication) also seems to be finding $f \sim 10\%$. Although these other surveys are not yet characterized in the literature, it does appear that our high fraction of distant TNOs is not out of line with that being produced by other groups since the start of 1999; there is thus no strong evidence for having reached the roll over in the size distribution.

To quantify this, we constructed a simple model of a TNO disk beginning at 40 AU and extending to infinity, characterized by a luminosity of slope α and a volume number density in the ecliptic declining radially as a power law with index β (see Gladman et al. 1998), and we examined the case of 16 detections (that in this work and our previous pencil-beam work). We computed analytically the probability that the most distant object in the sample would be at a given distance $R_{\max}$ (Fig. 10). Our detection of the most distant source, 1999 DG_8 at 61 AU, is in good agreement with the expectation from a steep luminosity function. The $\alpha = 0.52$ curves visually illustrate the "distant fraction" problem again: the probability that surveys with at least this many detections (the curves depend on N) would detect a most distant object at only 55–60 AU is relatively small. The lack of detections outside 55 AU in the surveys of Jewitt et al. (1998) and Allen et al. (2001) increases the evidence for a proposed drop in the surface density outside 48 AU. However, we are concerned by the fact that there is known to be a very large population of scattered-disk objects traversing this region; why are they not being detected in the 48–65 AU range? Careful modeling of the scattered disk to classical belt population ratio in a complex model of the flux-limited surveys is necessary, but knowing the orbital element distributions will be required in order to do this correctly.

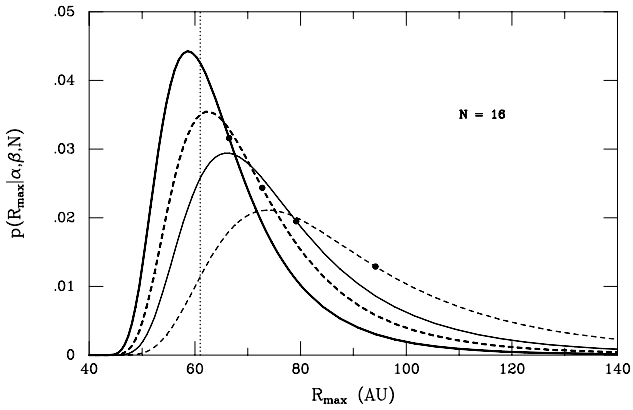

FIG. 10.—Probability distributions for the "most distant TNO." We created a disk model with a power-law heliocentric distance distribution of the form $r^{-\beta}$ (eq. [2] of G98) with an inner edge at $r = 40$ AU. For a sample of 16 objects with $r \geq 40$ AU, the curves show the probability that the most distant object in the sample will be at $R_{\max}$. Dashed curves indicate $\beta = -2$, solid curves are for $\beta = -3$. The two heavy curves are for $\alpha = 0.69$, and the two light curves for $\alpha = 0.52$ (bracketing published values). The light dot on each curve marks the expectation value of the distribution. The vertical dotted line marks the heliocentric distance at which we detected 1999 DG_8.

Thus, only since early 1999 have observations probed the $r > 48$ AU region; the dynamical state of this region will only be established with certainty over the coming 2–3 years as the known objects are recovered and others discovered. Ruling out the existence of distant TNOs on nearly circular orbits should require that several TNOs at aphelia of $a < 48$ orbits are observed and tracked in this region *without* the detection of low-e orbits, ensuring a bias-free view of that region. Unfortunately, many of the $r > 50$ AU TNOs have been lost.

9. SUMMARY

Kuiper Belt studies are yielding a bonanza of insights into the origin of the outer solar system. Our conclusions are as follows:

1. Our deep imaging surveys have discovered the first objects in the "distant" Kuiper Belt exterior to a heliocentric distance of 48 AU, with the fraction of such distant objects (10%–20%) in line with that expected for a smooth disk continuing into this region. This fraction seems to be replicated by the MPC-designated TNOs from other groups.

2. The size distribution appears to remain steep, $q \gtrsim 4$, all the way down to the 50 km diameter expected from accretional/collisional studies. Accretional modeling calculations then imply that planetesimal building proceeded unimpeded for timescales of at least ~ 10 Myr before the inner Kuiper Belt was dynamically excited to its present state.

3. A roll over to a flatter size distribution is expected somewhere in the $D = 5$–50 km range, which can only be probed with even deeper observations. The disk mass in the observed region out to ~ 60 AU is $\sim 0.1\ M_\oplus$, only weakly dependent on the roll-over size and radial distribution.

4. The dynamical state of the observed portions of the belt is heavily perturbed by violent dynamical processes, which further observations, especially in the distant belt outside 48 AU, will help to characterize. The ensemble of processes hypothesized in the literature are best tested in this region.

We are grateful to our CFHT telescope operator, Marie-Claire Hainaut, for sitting through the boredom of 7 hours a night observing the same field. We thank Brian Marsden for many exchanges regarding orbital parameters, as well as Hal Levison and Scott Tremaine for discussions. This work was supported by a Henri Chrétien international research grant (AAS), by NASA Origins grants NAG 5-8198 and NAG 5-9678, by an ACI Jeune award from the French Research Ministry, and an Observatoire de la Côte d'Azur BQR grant. A. M. thanks CNRS-INSU for travel support.

REFERENCES

Allen, R. L., Bernstein, G. M., & Malhotra, R. 2001, ApJ, 549, L241
Appenzeller, I., et al. 1998, Messenger, 94, 1
Beckwith, S. V. M., Henning, T., & Nakagawa, Y. 2000, in Protostars and Planets IV, ed. V. Mannings, A. P. Boss, & S. S. Russell (Tucson: Univ. Arizona Press), 533
Bernstein, G., & Khushalani, B. 2000, AJ, 120, 3323
Brown, M. J. I., & Webster, R. L. 1998, Publ. Astron. Soc. Australia, 15, 176 (BW98)
Brunini, A., & Melita, M. D. 1998, Icarus, 135, 408
Chiang, E. I., & Brown, M. E. 1999, AJ, 118, 1411 (CB99)
Cochran, A. L., Levison, H. F., Stern, S. A., & Duncan, M. J. 1995, ApJ, 455, 342 (C95)
Cohen, C. J., & Hubbard, E. C. 1965, AJ, 70, 10
Cuillandre, J.-C., Luppino, G. A., Starr, B. M., & Isani, S. 2000, in Optical Detectors for Astronomy II, ed. P. Amico & J. W. Beletic (Boston: Kluwer), 93
Davis, D. R., & Farinella, P. 1997, Icarus, 125, 50
Davis, D. R., Farinella, P., & Weidenschilling, S. J. 1999, in Lunar and Planetary Science XXX (Houston: Lunar Planet. Inst.), No. 1883
Delsanti, A. C., Hainaut, O., Boehnhardt, H., Delahodde, C. E., Sekiguchi, T., & West, R. M. 1999, BAAS, 31, Div. Planet. Sci. abstr. No. 26.03
Dohnanyi, J. S. 1969, J. Geophys. Res., 74, 2531
Dones, L. 1997, in ASP Conf. Ser. 122, From Stardust to Planetesimals, ed. Y. J. Pendleton & A. G. G. M. Tielens (San Francisco: ASP), 347
Duncan, M. J., & Levison, H. F. 1997, Science, 276, 1670
Duncan, M. J., Levison, H. F., & Budd, S. M. 1995, AJ, 110, 3073
Elliot, J. L., Kern, S. D., Millis, R. L., Buie, M. W., Wasserman, L. H., & Wagner, R. M. 2000, BAAS, 32, Div. Planet. Sci. abstr. No. 20.02
Fernández, J. A. 1978, Icarus, 34, 173
Fernández, J. A., & Brunini, A. 2000, Icarus, 145, 580
Fernández, J. A., & Ip, W.-H. 1984, Icarus, 58, 109
Gladman, B. 1998, Nature, 396, 513
———. 2001, Highlights Astron., in press
Gladman, B., & Duncan, M. 1990, AJ, 100, 1680
Gladman, B., Holman, M., Grav, T., Kavelaars, J., Nicholson, P., Aksnes, K., & Petit, J.-M. 2001, Icarus, submitted (astro-ph/0103435)
Gladman, B., & Kavelaars, J. J. 1997, A&A, 317, L35
Gladman, B., Kavelaars, J. J., Nicholson, P. D., Loredo, T. J., & Burns, J. A. 1998, AJ, 116, 2042 (G98)
Gomes, R. S. 2000, AJ, 120, 2695
Guillot, T., & Gladman, B. 2000, in ASP Conf. Ser. 219, Disks, Planetesimals, and Planets, ed. F. Garzón, C. Eiroa, D. de Winter, & T. J. Mahoney (San Francisco: ASP), 475
Hahn, J. M. 2000, in Lunar and Planetary Science XXXI (Houston: Lunar Planet. Inst.), No. 1797
Hahn, J. M., & Brown, L. 1999, in Lunar and Planetary Science XXX (Houston: Lunar Planet. Inst.), No. 1888
Hahn, J. M., & Malhotra, R. 1999, AJ, 117, 3041
Hainaut, O., West, R. M., Smette, A., & Marsden, B. G. 1994, A&A, 289, 311
Hayashi, C., Nakazawa, K., & Nakagawa, Y. 1985, in Protostars and Planets II, ed. D. C. Black & M. S. Matthews (Tucson: Univ. Arizona Press), 1100
Hollenbach, D. J., Yorke, H. W., & Johnstone, D. 2000, in Protostars and Planets IV, ed. V. Mannings, A. P. Boss, & S. S. Russell (Tucson: Univ. Arizona Press), 401
Holman, M. J. 1997, Nature, 387, 785
Holman, M. J., & Wisdom, J. 1993, AJ, 105, 1987
Ida, S., Bryden, G., Lin, D. N. C., & Tanaka, H. 2000a, ApJ, 534, 428
Ida, S., Larwood, J., & Burkert, A. 2000b, ApJ, 528, 351
Irwin, M., Tremaine, S., & Żytkow, A. N. 1995, AJ, 110, 3082 (ITZ95)
Jewitt, D., Luu, J., & Chen, J. 1996, AJ, 112, 1225 (JLC96)
Jewitt, D., Luu, J., & Trujillo, C. 1998, AJ, 115, 2125 (JLT98)
Jewitt, D. C., & Luu, J. X. 2000, in Protostars and Planets IV, ed. V. Mannings, A. P. Boss, & S. S. Russell (Tucson: Univ. Arizona Press), 1201
Kavelaars, J., Gladman, B., Petit, J.-M., Holman, M., Morbidelli, A. 2001, in preparation
Kenyon, S. J., & Luu, J. X. 1999, ApJ, 526, 465
Kortenkamp, S. J., & Wetherill, G. W. 2000, Icarus, 143, 60
Kowal, C. T. 1989, Icarus, 77, 118
Landolt, A. U. 1992, AJ, 104, 340
Larsen, J. A., et al. 2001, AJ, 121, 562
Lecar, M., & Franklin, F. A. 1973, Icarus, 20, 422
Levison, H. F. 1996, in ASP Conf. Ser. 107, Completing the Inventory of the Solar System, ed. T. W. Retting & J. M. Hahn (San Francisco: ASP), 173
Levison, H. F., & Duncan, M. J. 1990, AJ, 100, 1669 (LD90)
———. 1993, ApJ, 406, L35
———. 1997, Icarus, 127, 13
Levison, H. F., Lissauer, J. J., & Duncan, M. J. 1998, AJ, 116, 1998
Levison, H. F., & Malhotra, R. 1998, IAU Circ. 7073
Luu, J., Marsden, B. G., Jewitt, D., Trujillo, C. A., Hergenrother, C. W., Chen, J., & Offutt, W. B. 1997, Nature, 387, 573
Luu, J. X., & Jewitt, D. C. 1998, ApJ, 502, L91
Malhotra, R. 1995, AJ, 110, 420
———. 1996, AJ, 111, 504
———. 1998, in Lunar and Planetary Science XXIX (Houston: Lunar Planet. Inst.), No. 1476
Morbidelli, A. 1997, Icarus, 127, 1
Morbidelli, A., Thomas, F., & Moons, M. 1995, Icarus, 118, 322
Morbidelli, A., & Valsecchi, G. B. 1997, Icarus, 128, 464
Nesvorný, D., & Roig, F. 2001, Icarus, 150, 104
Petit, J.-M., Morbidelli, A., & Valsecchi, G. B. 1999, Icarus, 141, 367
Sheppard, S. S., Jewitt, D. C., Trujillo, C. A., Brown, M. J. I., & Ashley, M. C. B. 2000, AJ, 120, 2687
Stern, S. A., & Colwell, J. E. 1997a, AJ, 114, 841
———. 1997b, ApJ, 490, 879
Thommes, E. W., Duncan, M. J., & Levison, H. F. 1999, Nature, 402, 635
Torbett, M. V. 1989, AJ, 98, 1477
Torbett, M. V., & Smoluchowski, R. 1990, Nature, 345, 49
Trilling, D. E., Brown, R. H., & Rivkin, A. S. 2000, ApJ, 529, 499
Trujillo, C. A., Jewitt, D. C., & Luu, J. X. 2000, ApJ, 529, L103
Wuchterl, G., Guillot, T., & Lissauer, J. J. 2000, in Protostars and Planets IV, ed. V. Mannings, A. P. Boss, & S. S. Russell (Tucson: Univ. Arizona Press), 1081